Investigation of Structured Green-Band Emission and Electron−Phonon Interactions in Vertically Aligned ZnO Nanowires

Rui Chen,[†] Yeeyan Tay,[‡] Jun Ye,[‡] Yang Zhao,[‡] Guozhong Xing,[†] Tom Wu,[†] and Handong Sun*,[†]

Division of Physics and Applied Physics, School of Physical and Mathematical Sciences, Nanyang Technological University, Singapore 637371, Singapore, and Division of Materials Science, School of Materials Science and Engineering, Nanyang Technological University, Singapore 639798, Singapore

Received: July 12, 2010; Revised Manuscript Received: September 2, 2010

We have investigated the green band (GB) emission from vertically aligned ZnO nanowires (NWs) prepared by vapor−liquid−solid growth technique. At low temperatures, the GB emission consists of two sets of zero phonon lines and their phonon replicas independent of the laser excitation power. Temperature-dependent photoluminescence (PL) measurement is performed at temperatures from 10 to 300 K, and the thermal evolution of peak widths and the origin of PL quenching at high temperatures are discussed in detail. The multimode Brownian oscillator model is adopted to reproduce the structured GB and to determine the Huang−Rhys factor. It is found that the two electronic transitions are strongly coupled to different LO phonon modes, and the size-dependent electron−phonon coupling strength is examined.

I. Introduction

Wurtzite ZnO, a wide-band gap (3.37 eV) polar semiconductor, is recognized as one of the most promising materials for ultraviolet light-emitting devices and laser diodes.[1,2] Compared with other wide-band gap materials, ZnO has the advantage of a large exciton binding energy (∼60 meV) at room temperature. Clear understanding of various optical properties of ZnO is crucial for full exploitation of this material for optoelectronic applications. Until now, various deep-level emissions reported are related to intrinsic or extrinsic defects such as zinc vacancies (V_{Zn}),[3] interstitial zinc (Zn_i),[4] oxygen vacancies (V_O),[5,6] and interstitial oxygen (O_i).[7–9] Among them, there is an emission band located at around 2.45 eV, called the green band (GB), which is as well known as the yellow band in GaN.[10] This GB emission often includes two sets of phonon progressions with the same longitudinal optical (LO) mode. This characteristic has been observed in various samples such as ZnO bulk crystal,[11–13] microrock,[14] or nanowires (NWs).[15] However, to date, there are still controversies regarding the origin of this GB emission and its fine structures. The model on the divalent copper ion Cu^{2+} on a zinc lattice site of ZnO proposed by Dingle[11] and later discussed by Garces et al.[13] has received much attention. However, Reynolds et al.[12] suggested that transitions from the two shallow donor states to the same deep acceptor level are partially responsible for the fine structure of the GB emission. On the other hand, electron−phonon interactions are important, especially in polar semiconductors. From the viewpoint of spectral simulation, several approaches have been employed to discuss the Huang−Rhys factor, for example, a vibronic model including two donors and one deep acceptor,[12] a simple fitting with a Poisson distribution,[16] and the multimode Brownian oscillator (MBO) model.[17] The MBO model is preferable because it can effectively reproduce the structured GB emission and provides accurate parameters for further discussion.

In this work, a systematic investigation of the structured GB emission in ZnO NWs was carried out for the first time to reach a better understanding of the optical properties of this material in low dimension. Characteristics of the structured GB emission were examined through detailed power-dependent and temperature-dependent photoluminescence (PL) measurements performed at temperatures between 10 and 300 K. At the same time, the MBO model was adopted to investigate the electron−phonon interactions with the consideration of a thermal bath. This allows various size-dependent properties to be discussed in comparison to the bulk counterpart.

II. Experimental Procedures

The sample used herein is highly vertically aligned ZnO NWs grown on *c*-plane sapphire substrates by using vapor phase transport via the vapor−liquid−solid mechanism.[18] The substrates were carefully cleaned before any treatments. Gold films with a nominal thickness of 2 nm were deposited on the substrates before the growth and then annealed at 800 °C for 4 min to form Au nanoparticles as catalyst. A mixture of high-purity ZnO powder (99.999%) and graphite powder (99.999%) with a weight ratio of 1:1 ZnO/C was used as the source. The growth was performed at 950 °C for 15 min, and high-purity argon mixed with 5% oxygen with a constant flow rate of 50 sccm was used as the carrying gas.

Morphological characterization was performed with a JEOL JSM-6700F field emission scanning electron microscope (FESEM). The PL measurements were performed between 10 and 300 K within a closed-cycle helium cryostat. A cw He−Cd laser emitting at 325 nm was used as the PL excitation source, and the signal was dispersed by a 750 mm monochromator combined with suitable filters and detected by a photomultiplier by using the standard lock-in amplifier technique.

* To whom correspondence should be addressed. E-mail: hdsun@ntu.edu.sg.
[†] School of Physical and Mathematical Sciences.
[‡] School of Materials Science and Engineering.

10.1021/jp1064209
Published on Web 09/22/2010

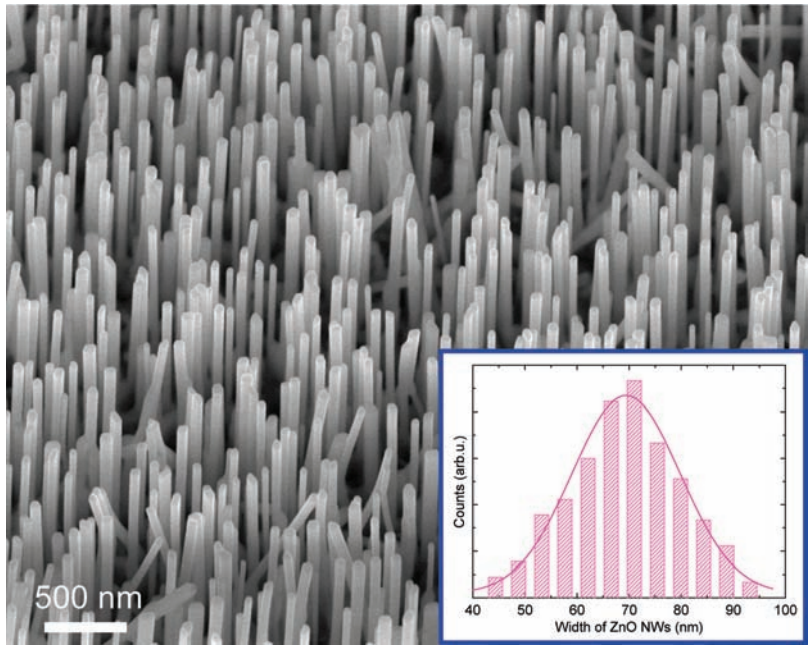

Figure 1. SEM image of the as-grown vertially aligned ZnO NWs. The inset is the width histograms of the sample.

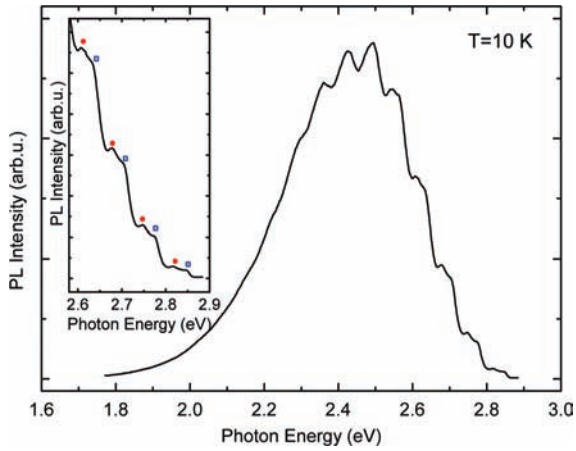

Figure 2. Low-temperature (10 K) PL emission of the ZnO NWs. The inset is the enlarged portion of the high-energy region.

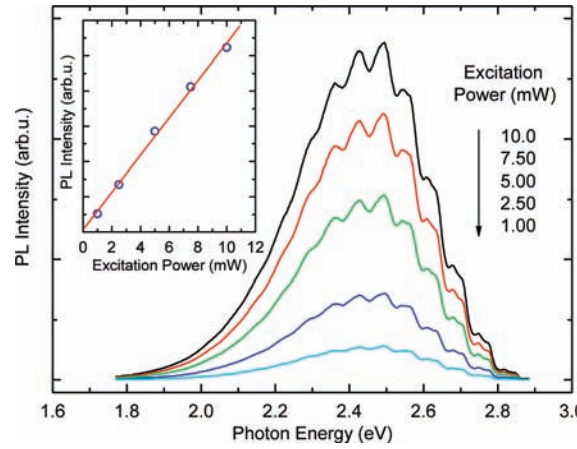

Figure 3. PL spectra taken at low temperature (10 K) as a function of excitation powers. The inset is the integrated PL intensity with the change of excitation power.

III. Results and Discussion

A. Characteristics of the Structured GB Emission. Figure 1 shows a typical SEM image of as-grown ZnO NWs, and the inset is the width histogram of the sample. The as-grown samples are vertically aligned NW arrays, and the ZnO NWs show very uniform diameters (70 ± 10 nm). The X-ray diffraction results (not shown here) indicate that the ZnO NWs are grown with a *c*-axis orientation.

Figure 2 depicts the low-temperature (10 K) visible-range PL spectra of ZnO NWs under laser power around 3.7 mW. The inset is an enlarged portion of the spectrum in the high-energy range. As shown in Figure S1 in the Supporting Information, at low temperatures, the sample is dominated by emission from donor-bound exciton complexes (BECs) located at 3.352 eV. Other peaks at 3.372 eV related to the free exciton (FX),and the LO phonon replica of the BECs and FX are also observed.[19] In this paper, we will focus our investigation on the visible PL signal, and the near-band emission will not be discussed here. As shown in Figure 2, the GB emission consists of a broad-band emission with two sets of fine structures indicated by opened circles and closed squares in the inset. The zero phonon lines (ZPLs) of the two series are located at around 2.85 and 2.82 eV, respectively, with an energy spacing of about 30 meV. Any two adjacent lines in the fine structure of each series are separated by about 71 meV, a spacing close to the LO phonon energy of ZnO and consistent with the values reported in the pervious research.[20] The fine structure is more obvious in the high-energy region and gradually fades out at the low-energy side.

To further investigate the structured GB emission, we performed PL measurements under various excitation intensities at low temperatures. Figure 3 shows the dependence of the PL spectra on the excitation intensity for the ZnO NWs at 10 K. It is noted that for an excitation power ranging from 1 to 10 mW, the fine structures maintained the same energy position without shifting. In fact, spectra of various powers overlap after proper normalizations. The inset of Figure 3 is the integrated PL intensity as a function of the excitation power. In the power window of interest, the PL intensity has a linear relation with the excitation power. The apparent phonon progressions and the 30 meV energy spacing between the two sets of fine structures indicate that there may exist two electronic transitions strongly coupled to the LO phonons.

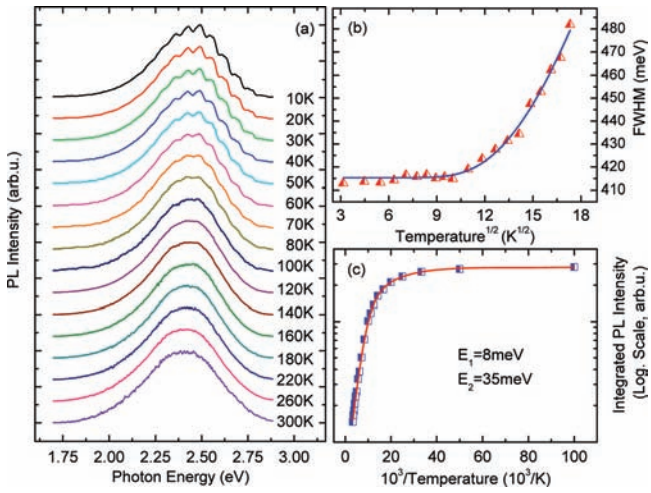

Figure 4. (a) Normalized temperature-dependent PL spectra from 10 to 300 K. (b) Peak widths as a function of temperature. The solid curve is the fitting according to eq 1. (c) Integrated PL intensity with the change of temperature. The solid curve is the fitting according to eq 2.

To probe the physical origin of the structured GB emission and examine its temperature dependence, the PL measurement was carried out in the temperature range from 10 to 300 K with a laser power of 3.7 mW, and the normalized spectra are presented in Figure 4a. The maximum intensity of the broad GB emission band is fixed at a certain energy for various temperatures, and the fine structures of the LO-phonon replica gradually fade out with rising temperature. At room temperature, the entire GB emission becomes a broad, smooth band. A detailed discussion of the temperature-induced spectral changes will be given later along with the introduction of the MBO model.

Figure 4b shows the overall full width at half maximum (fwhm) as a function of $T^{1/2}$. The width is found to be 415 meV at temperatures lower than 100 K and monotonically increase with temperature.[21] The characteristics are similar to a previous investigation,[14] which can be ascribed to the deep acceptor state of Cu^{2+} ions with $3d^9$ configuration proposed by Dingle.[11] Therefore, the width of the emission band changing with temperature can be described by the expression below derived from the configuration coordinate (CC) model,[22]

$$W(T) = W(0)\sqrt{\coth\left(\frac{\hbar w^{e}}{2k_{B}T}\right)} \tag{1}$$

where $W(0)$ is the peak width at low temperatures, $\hbar w^e$ is the energy of the effective vibrational mode in the excited state of the defect, and k_B is the Boltzmann constant. The blue line in Figure 4b is the corresponding fitting obtained by using eq 1. From the best fit to the experimental data on the temperature variation of the peak width, we found $W(0) = 415$ meV and $\hbar w^e = 50.5$ meV. The calculated vibrational energy is close to the previously reported value.[14]

Next, we discuss the temperature dependence of the integrated PL intensity. Relevant information is presented in Figure 4c. There is a gradual decrease in the integrated PL intensity with increasing temperature, which is a common feature of semiconductors due to the thermal activation of nonradiative centers or thermal escaping of carriers involved in the emission process. As a matter of fact, the temperature-dependent integrated PL intensity cannot be well fitted by using an Arrhenius plot with a single thermal activation but can be adequately described by the following dual activation energy model,[23,24]

$$I(T) = \frac{I(0)}{[1 + c_1\exp(-E_1/k_BT) + c_2\exp(-E_2/k_BT)]} \tag{2}$$

where E_1 and E_2 denote different activation energies for two different thermal-activation processes, and the parameters c_1 and c_2 are the relative ratios of nonradiative recombination and reflect the competition between recapture and nonradiative recombination. From a least-squares fitting procedure performed by using eq 2, the activation energies obtained are estimated to be 8 and 35 meV, respectively. The former activation energy is significantly lower and can be ascribed to the temperature-dependent capture cross section of the carriers at the recombination centers,[25] whereas the latter one corresponds to the thermal dissociation energy required for the nonradiative recombination of the electron from the excited state to the ground state.[26]

B. MBO Fitting and Electron−Phonon Interactions. The GB emission can be well described by the MBO model, a theoretical framework to treat the coupling of nuclear coordinates to optical excitations and electronic relaxation channels in solids. We consider an electronic two-level system with some primary nuclear coordinates coupled linearly to it and to a harmonic bath. The primary phonons can be those of host medium or pseudolocalized modes associated with the guest atoms or molecules.[27−29] The Hamiltonian of the system is given by,

$$H = |g\rangle H_g\langle g| + |e\rangle H_e\langle e| + H' \tag{3}$$

where

$$H_g = \sum_j \left[\frac{p_j^2}{2m_j} + \frac{1}{2}m_j\omega_j^2 q_j^2\right] \tag{4}$$

$$H_e = \hbar\omega_{eg}^0 + \sum_j \left[\frac{p_j^2}{2m_j} + \frac{1}{2}m_j\omega_j^2(q_j + d_j)^2\right] \tag{5}$$

$$H' = \sum_n \left[\frac{P_n^2}{2m_n} + \frac{1}{2}m_n\omega_n^2\left(Q_n - \sum_j \frac{c_{nj}q_j}{m_n\omega_n^2}\right)^2\right] \tag{6}$$

Here, $p_j(P_n)$, $q_j(Q_n)$, $m_j(m_n)$, and $\omega_j(\omega_n)$ are the momentum, the coordinate, the mass, and the angular frequency of the j^{th} (n^{th}) nuclear mode of the primary (bath) oscillators, respectively. d_j represents the displacement for the j^{th} nuclear mode in the excited electronic state. $\hbar\omega_{eg}^0$ is the energy separation of the purely electronic levels. H' describes the bath modes and their coupling to the primary oscillators with a coupling strength c_{nj}. The cross terms in q_jQ_n are responsible for damping.[30]

The key parameters of the MBO model are the frequencies of the primary oscillators ω_j, the damping coefficient γ that controls the coupling strength of the primary oscillator and the bath modes, and the Huang−Rhys factor S which reflects the electron−phonon coupling strength. Here, we take the LO phonon as the only primary phonon in the model; that is, $\omega_j = \omega_{LO}$. The LO phonon frequency ω_{LO} is assigned to be the

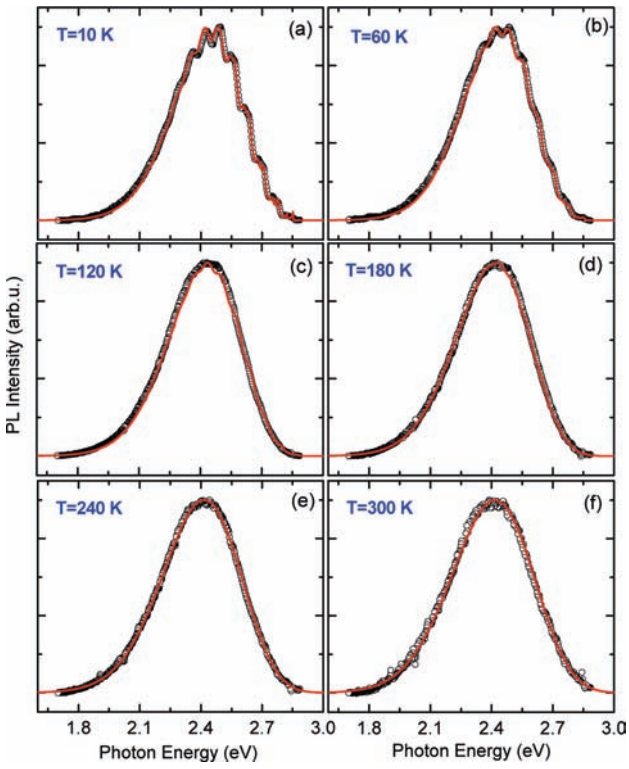

Figure 5. PL spectra taken at various temperatures (open circles) and spectra (red curves) obtained by the MBO model.

spacing between adjacent phonon side bands. Then, the PL line shape can be calculated from

$$I_{PL} = \frac{1}{\pi}\mathrm{Re}\int_0^\infty \exp[i(\omega - \omega_{eg} + \lambda)t - g^*(t)]\,\mathrm{d}t \quad (7)$$

where $\lambda = S\hbar\omega_{LO}$ and $g^*(t)$ is the complex conjugate of the line broadening function $g(t)$

$$g(t) = \frac{1}{2\pi}\int_{-\infty}^{\infty} d\omega \frac{C''(\omega)}{\omega^2}[1 + \coth(\beta\hbar\omega/2)](e^{-i\omega t} + i\omega t - 1) \quad (8)$$

where $\beta = 1/k_B T$. The spectral response function for a Markovian bath, which is coupled with the primary oscillator of frequency ω_{LO} with a damping factor γ linearly, can be expressed as

$$C''(\omega) = \frac{2\lambda\omega_{LO}^2\omega\gamma}{\omega^2\gamma^2 + (\omega_{LO}^2 - \omega^2)^2} \quad (9)$$

Here, we simulate the structured GB emission of ZnO NWs at various temperatures by considering that the spectrum is composed of two electronic transitions. Figure 5 displays the PL spectra (open circles) of the ZnO NWs measured at various temperatures, and the red lines are the spectra simulated by using the MBO model. The parameters used for fitting are listed in Table 1, where the ratio column lists the weight coefficients for the two transitions in the calculated curve. The sensitivity of the model parameters to the spectrum features can be seen in Figure S2 in the Supporting Information. As depicted in Figure 5, a good fitting was obtained. A few observations can be made from the MBO fitting for the GB emission. First, we note that there are two kinds of active LO phonon modes (ω_1 = 563.43 cm^{-1} and ω_2 = 574.1 cm^{-1}) needed to produce a high-quality fit, at variance with previous reports with only one phonon mode.[16,17] It is well known that the LO phonons of ZnO single crystal have a 574 cm^{-1} A1-LO component and a 583 cm^{-1} E1-LO component.[31] We note that the difference (~10.7 cm^{-1}) of the two LO modes used in the MBO fitting are similar to that of the single crystal (~9 cm^{-1}). Thus, we ascribe the two LO phonon modes to the A1-LO and E1-LO components of the ZnO phonons. It is important to note that, as compared with bulk ZnO, smaller values of the phonon energies may result from the phonon zone-folding effect because of a small NW diameter.[32] Second, at 10 K, it is also found that γ_1 and γ_2 are 65 and 60 cm^{-1} for the bulk ZnO, respectively,[17] whereas our experimental result shows that γ_1 and γ_2 are 70 and 75 cm^{-1}, respectively. Reduced sizes of the NWs (as compared to the bulk ZnO) will lead to a higher concentration of the surface defects, which have direct interactions with the environment matrix, thus resulting in an increase of the coupling between the primary oscillators and the secondary bath oscillators.[33,34] Third, the size of NWs affects the value of the electron−phonon coupling strength. S at 10 K is 6.05, which is much smaller compared to 6.4−6.9 reported for the bulk ZnO material.[12,13,16,17] Detailed spectrum comparison of the ZnO NWs and bulk ZnO can be found in Figure S3 in the Supporting Information. Similar characteristics have also been observed in other low-dimensional material system, such as Ce^{3+}-doped yttrium aluminum garnet nanophosphors[35] and ZnO/ZnMgO multi quantum wells.[36,37] Fourth, from Table 1, we can note that the electron−phonon coupling strength increases with raising temperature, which leads to thermal broadening of each vibronic transition. From the result of MBO modeling, the two ZPLs at 10 K are located at 2.822 and 2.852 eV, far below the band gap of ZnO, implying that the structured GB emission is related to the deep-level emission such as substitutional Cu^{2+} on the zinc site as proposed by Dingle.[11] At the same time, determination of the γ and S factors from the experimental results enables us to determine the size-dependent characteristics of ZnO NWs.

IV. Conclusions

We have investigated the characteristics of structured GB emission from vertically aligned ZnO NWs by detailed optical spectroscopy as well as with the MBO analysis. Our results indicate that the structured GB emission can be attributed to two electronic transitions that are related to the deep acceptor

TABLE 1: Parameters Used for MBO Fitting at Various Temperatures

temperature (K)	γ_1 (cm^{-1})	ω_1 (cm^{-1})	S_1	ZPL-1 (eV)	γ_2 (cm^{-1})	ω_2 (cm^{-1})	S_2	ZPL-2 (eV)	Ratio 1/2
10	70	563.43	6.05	2.822	75	574.1	6.05	2.852	0.5
60	75		6.15	2.822	80		6.15	2.852	
120	75		6.55	2.842	80		6.55	2.872	
180	75		6.75	2.842	80		6.75	2.872	
240	75		7.2	2.872	80		7.2	2.902	
300	75		7.3	2.882	80		7.3	2.912	

levels with a strong electron−phonon coupling strength. Results from our modeling demonstrate convincingly that the electron−phonon coupling strength is much smaller than that in bulk material, which points out an approach to reduce the unwanted electron−phonon interaction in optoelectronic devices.

Acknowledgment. Support from the Singapore Ministry of Education through the Academic Research Fund (Tier 1) under Project No. RG40/07 and from the Singapore National Research Foundation through the Competitive Research Programme (CRP) under Project No. NRF-CRP5-2009-04 is gratefully acknowledged.

Supporting Information Available: Figure S1, entire luminescence spectrum of ZnO NWs at 10 K; Figure S2, spectrum features change with MBO model parameters, such as S, γ, and ω_{LO}; Figure S3, low-temperature structured GB emission from ZnO NWs and ZnO bulk. This material is available free of charge via the Internet at http://pubs.acs.org.

References and Notes

(1) Tang, Z. K.; Wong, G. K. L.; Yu, P.; Kawasaki, M.; Ohtomo, A.; Koinuma, H.; Segawa, Y. *Appl. Phys. Lett.* **1998**, *72*, 3270.
(2) Tsukazaki, A.; Ohtomo, A.; Onuma, T.; Ohtani, M.; Makino, T.; Sumiya, M.; Ohtani, K.; Chichibu, S. F.; Fuke, S.; Segawa, Y.; Ohno, H.; Koinuma, H.; Kawasaki, M. *Nat. Mater.* **2005**, *4*, 42.
(3) Zeng, H.; Li, Z.; Cai, W.; Liu, P. *J. Appl. Phys.* **2007**, *102*, 104307.
(4) Djurisic, A. B.; Leung, Y. H.; Tam, K. H.; Ding, L.; Ge, W. K.; Chen, H. Y.; Gwo, S. *Appl. Phys. Lett.* **2006**, *88*, 103107.
(5) Jeong, S. H.; Kim, B. S.; Lee, B. T. *Appl. Phys. Lett.* **2003**, *82*, 2625.
(6) Tam, K. H.; Cheung, C. K.; Leung, Y. H.; Djurisic, A. B.; Ling, C. C.; Beling, C. D.; Fung, S.; Kwok, W. M.; Chan, W. K.; Phillips, D. L.; Ding, L.; Ge, W. K. *J. Phys. Chem. B* **2006**, *110*, 20865.
(7) Djurisic, A. B.; Leung, Y. H.; Tam, K. H.; Hsu, Y. F.; Ding, L.; Ge, W. K.; Zhong, Y. C.; Wong, K. S.; Chan, W. K.; Tam, H. L.; Cheah, K. W.; Kwok, W. M.; Phillips, D. L. *Nanotechnology* **2007**, *18*, 095702.
(8) Ahn, C. H.; Kim, Y. Y.; Kim, D. C.; Mohanta, S. K.; Cho, H. K. *J. Appl. Phys.* **2009**, *105*, 013502.
(9) McCluskey, M. D.; Jokela, S. J. *J. Appl. Phys.* **2009**, *106*, 071101.
(10) Jenny, J.; Jones, R.; Van Nostrand, J. E.; Reynolds, D. C.; Look, D. C.; Jogai, B. *Solid State Commun.* **1998**, *106*, 701.
(11) Dingle, R. *Phys. Rev. Lett.* **1969**, *23*, 579.
(12) Reynolds, D. C.; Look, D. C.; Jogai, B. *J. Appl. Phys.* **2001**, *89*, 6189.
(13) Garces, N. Y.; Wang, L.; Bai, L.; Giles, N. C.; Halliburton, L. E.; Cantwell, G. *Appl. Phys. Lett.* **2002**, *81*, 622.
(14) Su, F. H.; Liu, Y. F.; Chen, W.; Wang, W. J.; Ding, K.; Li, G. H.; Joly, A. G.; McCready, D. E. *J. Appl. Phys.* **2006**, *100*, 013107.
(15) Hong, W. K.; Jo, G.; Choe, M.; Lee, T.; Sohn, J. I.; Welland, M. E. *Appl. Phys. Lett.* **2009**, *94*, 043103.
(16) Kuhnert, R.; Helbig, R. *J. Lumin.* **1981**, *26*, 203.
(17) Shi, S. L.; Li, G. Q.; Xu, S. J.; Zhao, Y.; Chen, G. H. *J. Phys. Chem. B* **2006**, *110*, 10475.
(18) Huang, M. H.; Wu, Y. Y.; Feick, H.; Tran, N.; Weber, E.; Yang, P. D. *Adv. Mater.* **2001**, *13*, 113.
(19) Sun, H. D.; Segawa, Y.; Kawasaki, M.; Ohtomo, A.; Tamura, K.; Koinuma, H. *J. Appl. Phys.* **2002**, *91*, 6457.
(20) Calleja, J. M.; Cardona, M. *Phys. Rev. B* **1977**, *16*, 3753.
(21) Li, J. W.; Yang, L. W.; Zhou, Z. F.; Chu, P. K.; Wang, X. H.; Zhou, J.; Li, L. T.; Sun, C. Q. *J. Phys. Chem. C* **2010**, *114*, 13370.
(22) Hwang, C. J. *Phys. Rev.* **1969**, *180*, 827.
(23) Chen, R.; Xing, G. Z.; Gao, J.; Zhang, Z.; Wu, T.; Sun, H. D. *Appl. Phys. Lett.* **2009**, *95*, 061908.
(24) Sun, H. D.; Calvez, S.; Dawson, M. D.; Gupta, J. A.; Aers, G. C.; Sproule, G. I. *Appl. Phys. Lett.* **2006**, *89*, 101909.
(25) Krustok, J.; Collan, H.; Hjelt, K. *J. Appl. Phys.* **1997**, *81*, 1442.
(26) Kim, J. H.; Park, D. S.; Yu, J. H.; Kim, T. S.; Jeong, T. S.; Youn, C. J. *J. Mater. Sci.* **2008**, *43*, 3144.
(27) Caldeira, A. O.; Leggett, A. J. *Ann. Phys.* **1983**, *149*, 374.
(28) Zhao, Y.; Knox, R. S. *J. Phys. Chem. A* **2000**, *104*, 7751.
(29) Lax, M. *J. Chem. Phys.* **1952**, *20*, 1752.
(30) Knox, R. S.; Small, G. J.; Mukamel, S. *Chem. Phys.* **2002**, *281*, 1.
(31) Damen, T. C.; Porto, S. P. S.; Tell, B. *Phys. Rev.* **1966**, *142*, 570.
(32) Chen, C. H.; Chen, Y. F.; Shih, A.; Lee, S. C.; Jiang, H. X. *Appl. Phys. Lett.* **2001**, *78*, 3035.
(33) Ye, J.; Zhao, Y.; Ng, N.; Cao, J. *J. Phys. Chem. B* **2009**, *113*, 5897.
(34) Cerullo, G.; De Silvestri, S.; Banin, U. *Phys. Rev. B* **1999**, *60*, 1928.
(35) Su, L. T.; Tok, A. I. Y.; Zhao, Y.; Ng, N.; Boey, F. Y. C.; Woodhead, J. L.; Summers, C. J. *J. Phys. Chem. B* **2008**, *112*, 10830.
(36) Sun, H. D.; Makino, T.; Tuan, N. T.; Segawa, Y.; Kawasaki, M.; Ohtomo, A.; Tamura, K.; Koinuma, H. *Appl. Phys. Lett.* **2001**, *78*, 2464.
(37) Sun, H. D.; Makino, T.; Segawa, Y.; Kawasaki, M.; Ohtomo, A.; Tamura, K.; Koinuma, H. *J. Appl. Phys.* **2002**, *91*, 1993.

JP1064209

Supporting Information

Investigation of Structured Green Band Emission and Electron-Phonon Interactions in Vertically Aligned ZnO Nanowires

Rui Chen, [‡] Yeeyan Tay, [†] Jun Ye, [†] Yang Zhao, [†] Guozhong Xing, [‡] Tom Wu, [‡] and Handong Sun [‡*]

[‡]*Division of Physics and Applied Physics, School of Physical and Mathematical Sciences, Nanyang Technological University, Singapore 637371, Singapore*

[†]*Division of Materials Science, School of Materials Science and Engineering, Nanyang Technological University, Singapore 639798, Singapore*

[*] To whom correspondence should be addressed, electronic mail: hdsun@ntu.edu.sg

1. The entire luminescence spectrum of ZnO NWs at low temperature

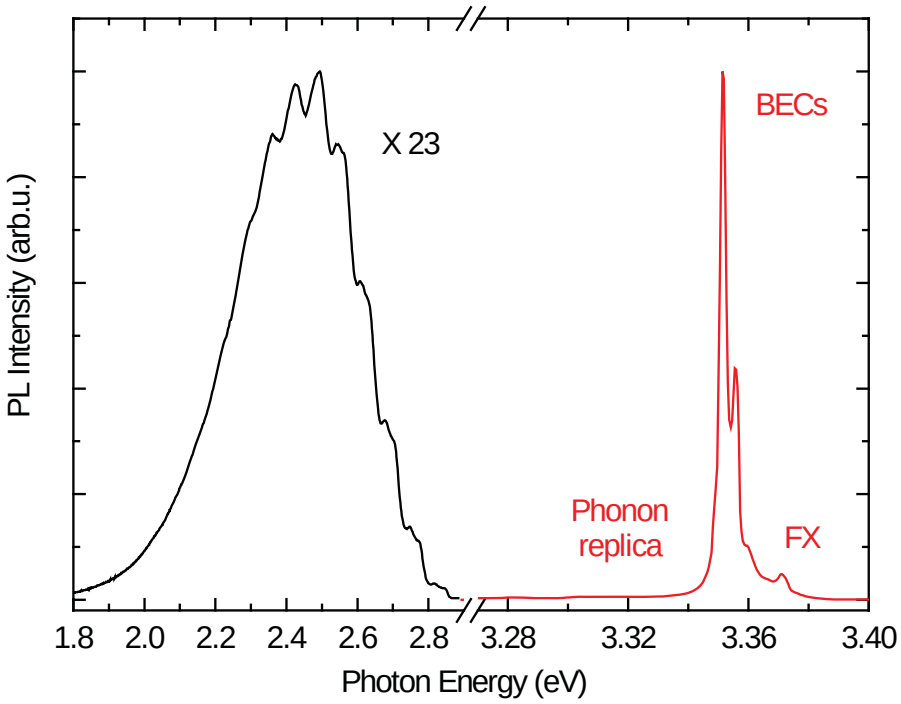

Figure S1. The entire luminescence spectrum of ZnO NWs at 10 K.

2. The sensitivity of MBO model calculation

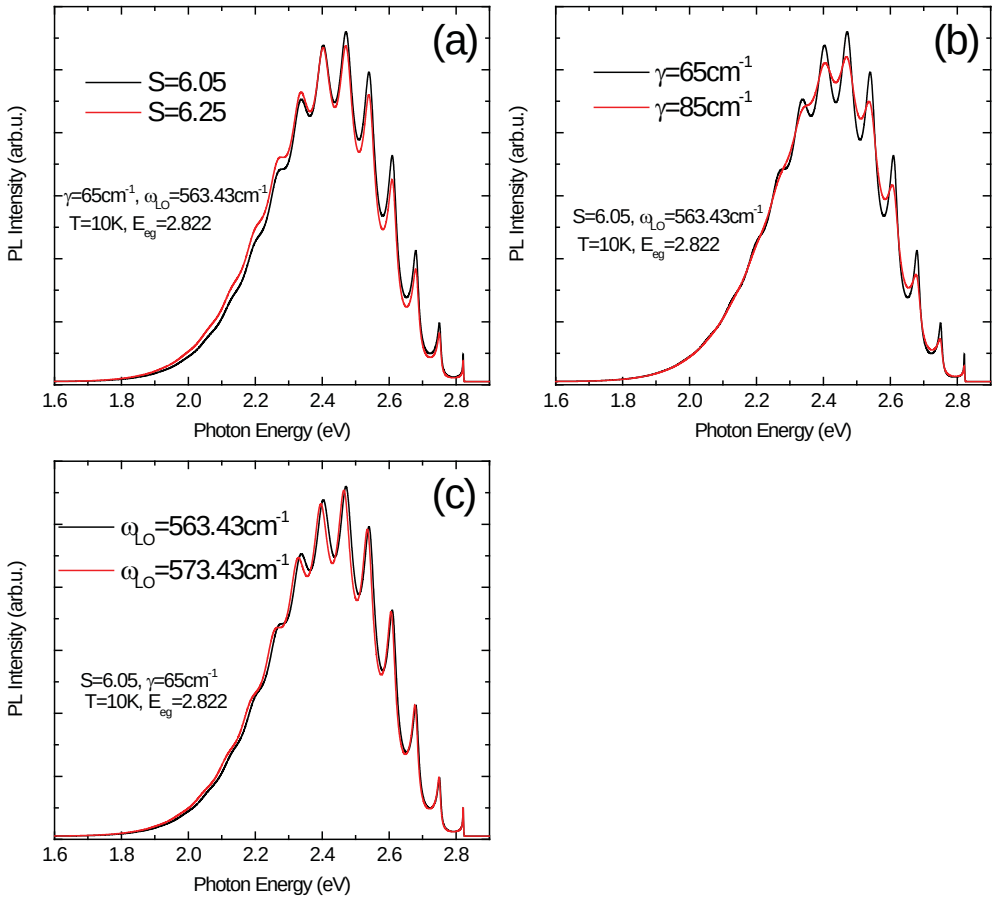

Figure S2. The spectrum features change with MBO model parameters, such as S, γ, and ω_{LO}, respectively.

3. The structured green band emission comparison between ZnO NWs and bulk

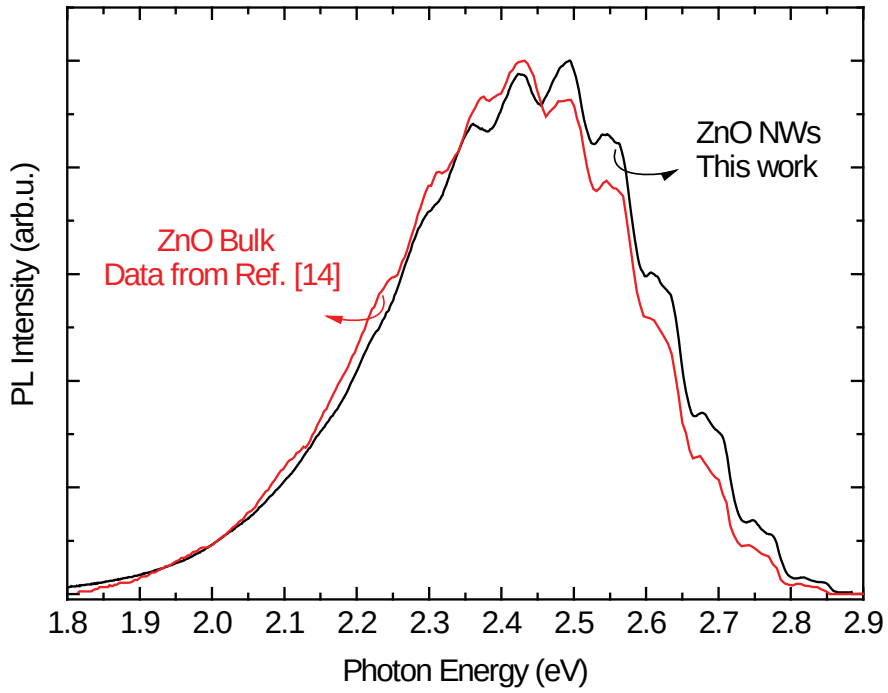

Figure S3. Low temperature structured green band emission from ZnO NWs and ZnO bulk.